Available online at www.sciencedirect.com
SCIENCE DIRECT
Brain Research 983 (2003) 23–35
BRAIN RESEARCH
www.elsevier.com/locate/brainres

Research report

Brain responses to micro-machined silicon devices

D.H. Szarowski[a,*], M.D. Andersen[a], S. Retterer[c], A.J. Spence[c], M. Isaacson[c], H.G. Craighead[c], J.N. Turner[a,b], W. Shain[a,b]

[a]*Wadsworth Center, New York State Department of Health, P.O. Box 509, Empire State Plaza, Albany, NY 12201-0509, USA*
[b]*Department of Biomedical Sciences, School of Public Health, The University at Albany, Albany, NY 12201-0509, USA*
[c]*School of Applied and Engineering Physics, Cornell University, Ithaca, NY 14853-2501, USA*

Accepted 15 May 2003

Abstract

Micro-machined neural prosthetic devices can be designed and fabricated to permit recording and stimulation of specific sites in the nervous system. Unfortunately, the long-term use of these devices is compromised by cellular encapsulation. The goals of this study were to determine if device size, surface characteristics, or insertion method affected this response. Devices with two general designs were used. One group had chisel-shaped tips, sharp angular corners, and surface irregularities on the micrometer size scale. The second group had rounded corners, and smooth surfaces. Devices of the first group were inserted using a microprocessor-controlled inserter. Devices of the second group were inserted by hand. Comparisons were made of responses to the larger devices in the first group with devices from the second group. Responses were assessed 1 day and 1, 2, 4, 6, and 12 weeks after insertions. Tissues were immunochemically labeled for glial fibrillary acidic protein (GFAP) or vimentin to identify astrocytes, or for ED1 to identify microglia. For the second comparison devices from the first group with different cross-sectional areas were analyzed. Similar reactive responses were observed following insertion of all devices; however, the volume of tissue involved at early times, <1 week, was proportional to the cross-sectional area of the devices. Responses observed after 4 weeks were similar for all devices. Thus, the continued presence of devices promotes formation of a sheath composed partly of reactive astrocytes and microglia. Both GFAP-positive and -negative cells were adherent to all devices. These data indicate that device insertion promotes two responses—an early response that is proportional to device size and a sustained response that is independent of device size, geometry, and surface roughness. The early response may be associated with the amount of damage generated during insertion. The sustained response is more likely due to tissue–device interactions.

Keywords: Brain response; Micro-machined silicon device; Tissue–device interaction; Cellular encapsulation

1. Introduction

The development of neuroprosthetic devices to restore nervous system function, lost due to trauma or disease, has been investigated for nearly three decades [1,2,16,22,23]. Such devices are becoming a practical reality in both the peripheral [9,20,21,30–32,45,46] and central nervous systems [3,7,10,13]. The most notable successes in humans are the alleviation of symptoms due to Parkinson's disease via deep brain stimulation [3,10,13] and deafness using cochlear implants [8]. It is clear that the application of neuroprosthetics, especially in the brain, would substantially benefit from miniaturization. For instance, in the human brain, target regions often have linear dimensions of only a few millimeters. Miniature neuroprosthetics have been fabricated using microfabrication technology developed by the integrated circuit industry [14,16,29,34]. Some of these devices have on-board electronics, including telemetry [24,26]. Others have been assembled into complex three-dimensional electrode arrays [14,25,26,29,34,37,43]. Typical dimensions for such devices range from 10 to 100s of micrometers making it possible to target specific regions of the brain.

The long-term function of these devices is limited due to cellular encapsulation that electrically and mechanically isolates the prosthesis from the brain [17,25,39,41,44]. This tissue response occurs following implantation of many materials other than silicon [2,30,42,46,47]. Encapsulation has generally been described by visualizing reactive gliosis, particularly the hypertrophy and increased expression of glial fibrillary acidic protein (GFAP) by

*Corresponding author. Tel.: +1-518-402-5233.
E-mail address: don@wadsworth.org (D.H. Szarowski).

0006-8993/03/$ – see front matter
doi:10.1016/S0006-8993(03)03023-3

astrocytes [11,18,28,33,35,40]. For times of 2 weeks and longer after implantation, we have demonstrated that astrocytes are a major cell type in the cellular sheath around inserted silicon devices [44]. This sheath is extremely dense and appears to contribute substantially to the electrical isolation of implants from the brain [44]. Preliminary results also suggest that microglia were also present [5].

The current study was designed to determine the effects of device features and insertion method on development of this cellular sheath. Reactive responses were compared following insertion of model devices with several cross-sectional areas of 16 900–1450 μm^2, devices with angular geometries and micrometer surface roughness, or rounded corners and very smooth surfaces. Some devices were inserted using a microprocessor-controlled instrument others were inserted by hand. Results from these experiments indicate that device size is the major contributing factor to size of the early response, while the sustained response is independent of any of these variables.

2. Methods

2.1. Device fabrication and preparation

Devices were fabricated at either the Cornell Nanofabrication Facility (CNF) at Cornell University or the Center for Neural Communication Technology (CNCT) at the University of Michigan. The former is an NSF-sponsored facility. The latter is an NIH, NCRR supported Resource Center. Devices fabricated at the CNF permitted us to alter design features. Devices fabricated at the CNCT have prescribed features and are produced for distribution to the general scientific community.

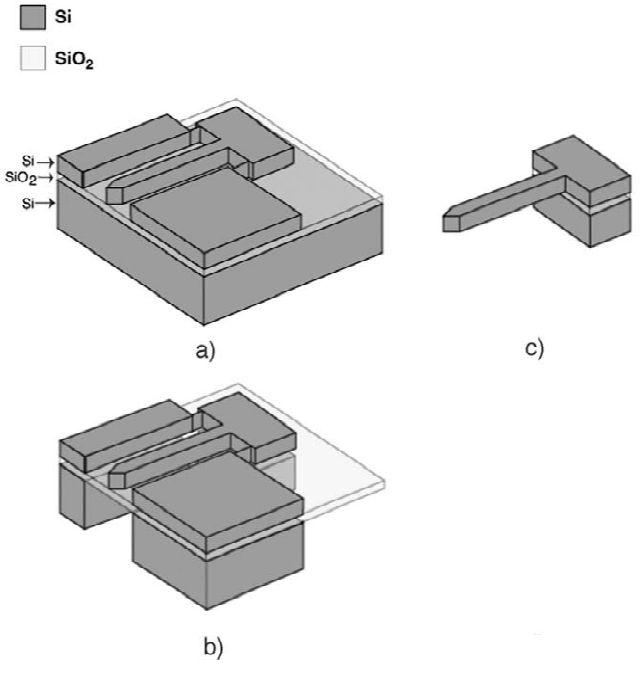

Fig. 1. Fabrication of CNF devices using reactive-ion etching. A cartoon demonstrating the steps required for fabrication of devices from SOI wafers.

Two different strategies were used for fabricating CNF devices. In the first, devices were micromachined from single crystal ⟨100⟩ silicon wafers (380-μm thick and 3 inches in diameter) using conventional silicon processing methods of photolithography and KOH etching as previously described [44]. In the second, devices were micromachined from silicon-on-insulator (SOI) wafers using conventional photolithography and deep reactive ion etching (Fig. 1A–C). SOI wafers contained a 50- or 100-μm thick silicon ‘device’ layer, a 1-μm thick buried oxide layer, and a 400-μm thick silicon ‘handle’ layer. A photoresist mask was patterned on the ‘device’ layer. An anisotropic deep reactive-ion ‘bosch’ etch removed the unmasked silicon, stopping at the buried oxide layer (Fig. 1A). Infra-red imaging was used to align the photoresist pattern of the ‘handle’ layer to features etched in the ‘device’ layer. A final ‘bosch’ etch of the handle layer yielded devices arranged on combs (Fig. 1B). The silicon oxide layer was removed with a hydrofluoric acid etch. Both methods produced a large number of uniform devices. KOH-etched devices had a 1×1-mm tab and a 2-mm long shaft (Fig. 2A). The cross-section of the shaft was trapezoidal (base=200 μm, top=60 μm; height=130 μm; inset Fig. 2A) corresponding to a cross-sectional area of 16 900 μm^2. SOI devices had somewhat different geometries. The tabs were cubes (500×500×500 μm). The 2-mm long shafts were 100-μm wide and had thickness of 50 or 100 μm depending on the thickness of the ‘device’ layer (Fig. 2B). The tips of these shafts were wedge shaped to form a sharp cutting edge for penetrating the pia and underlying brain tissue. The surfaces of the sides of the KOH-etched devices had micrometer-sized roughness. The sides and bottoms of the reactive-ion etched devices had smaller, ≤1 μm, irregularities not dissimilar to that observed on unpolished silicon surfaces.

CNCT devices (part # CN1.2) were obtained from the Center for Neural Communication Technology. The devices (Fig. 2C) had a 0.8×0.8-mm tab and a 2.08-mm long shaft. The cross-section of the shaft was a flattened ellipse (major axis=100–140 μm; thickness=15 μm; inset Fig. 2C) corresponding to a cross-sectional area of 1450–2500 μm^2. These devices had a rounded tip, and no sharp corners or discontinuities. From the tip, there were three regions of angular expansion to the full shaft width, and all surfaces were very smooth.

2.2. Device insertion

Devices were inserted 2 mm into the brain so that the bottom of the holding tabs rested on the brain surface.

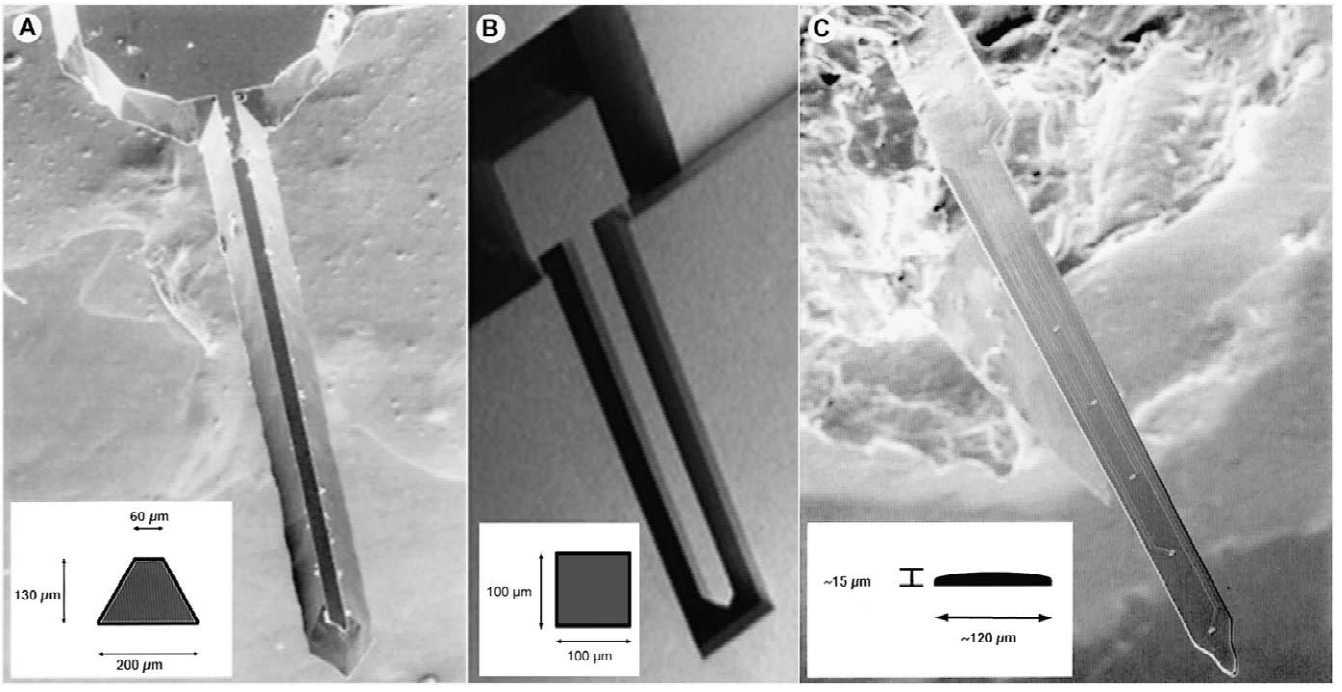

Fig. 2. Comparison of devices used in this study. SEM images show the CNF devices prepared by KOH etching (A) and RIE (B) and the CNCT device (C). The inserts associated with each SEM demonstrate their cross-section. The CNF, KOH-etched device has the largest cross-sectional area. The chisel shaped tip and surface irregularities of these devices are clearly visible. The CNF-RIE devices have shafts with rectangular cross-sections and more uniformity in their surfaces. Ridges frequently occur along the etched sides of these devices. The ridges are generated during the different cycles of the RIE and may have dimensions of up to several micrometers. The CNCT devices have smooth surfaces and rounded tips and edges.

CNF devices were inserted using our custom fabricated automated inserter [44]. CNCT devices were inserted by hand at rates similar to that used by the automated inserter. Adult (100–125 g) male Wistar and Sprague–Dawley rats were used. No differences were observed in the reactive responses of these two strains (data not shown). The automated inserter controls both insertion speed and penetration depth. Two different forceps held the CNF devices, and aligned them to the driving motion of the inserter. The forceps and precision drive table were mounted on a stereotaxic device, allowing accurate placement of CNF devices which were inserted into the right cerebral cortical hemisphere as previously described [44]. Briefly, rats (100–125 g) were anesthetized by intraperitoneal injection of tribromoethanol (targeted dose=23 mg/100 g body weight) or a mixture of Ketaset™ (targeted dose=2 mg/100 g body weight) and Xyla-Ject™ (targeted dose=0.25 mg/100 g body weight) and mounted in a stereotaxic animal holder. A small midline skin incision was made, the skin pulled aside, and a 2-mm burr hole made in the skull at a point 3-mm lateral and 3-mm distal from Bregma. After piercing the dura, the device was aligned above the hole in the bone and advanced until it just touched the surface of the brain. It was then retracted 1 mm and driven forward 3 mm (2-mm insertion into the brain) at a speed of 2 mm/s. This resulted in the device shaft being inserted into the cortex while the tab remained above the brain surface. CNCT devices were inserted manually using fine forceps to grip their tabs. Devices were aligned above the hole in the bone and inserted with a rapid, single motion into the cortex to the depth of the shaft. The tab and hole were covered with a piece of sterile dialysis tubing glued to the skull with Super Glue®. The skin was closed with wound clips and the animals were allowed to recover. All procedures were approved by the Wadsworth Center Institutional Animal Care and Use Committee.

2.3. Preparation of brain tissue for analysis

Animals were prepared for immunohistochemistry and conventional pathology 1 day and 1, 2, 4, 6, or 12 weeks after device insertion. At least two animals were used for each device type at each of the time points studied. The contralateral hemisphere served as a control for each animal. At the scheduled times, animals were anesthetized with tribromoethanol and perfusion fixed with 4% paraformaldehyde in 0.1 M phosphate buffer, pH7.4, using methods similar to those previously described [44]. Briefly, the skin and skull were removed and the devices were gently withdrawn from the tissue. The brains were then blocked in situ and the portion containing the device insertion site and the corresponding contralateral tissue were removed from the cranium. The tissue and devices were post-fixed for 24–48 h, and stored in Hepes-buffered Hanks saline (HBHS) containing sodium azide until

further processing. The tissue was sectioned using a vibratome. Coronal tissue slices (100-μm thick) were collected beginning at the brain surface and continuing for 2.5 mm. Tissue slices were stained for GFAP (sections 6 and 16), vimentin (sections 7 and 17), or ED1 (sections 5 and 15) to describe glial morphology and distribution.

For GFAP and vimentin, tissue slices were prepared for immunohistochemistry by treatment with 5% sodium borohydride, solubilized with 0.2% Triton X-100 in HBHS, and incubated with 0.1% bovine serum albumin (BSA) in HBHS to block non-specific binding, followed by rabbit anti-cow GFAP antibody (1:100 dilution, Sigma, St. Louis. MO, USA) or monoclonal mouse anti-vimentin antibody (1:100 dilution, Sigma) and rhodamine-labeled anti-rabbit IgG or anti-mouse antibody (1:100 dilution, Sigma). Samples were mounted in buffered glycerol saturated with *n*-propyl gallate in well slides prepared between two coverslips.

For ED1, tissue slices were treated as described above; however, after the BSA blocking step samples were incubated with 0.3% hydrogen peroxide in HBHS to block endogenous peroxidase. This incubation was followed by monoclonal mouse anti-ED1 antibody (1:50 dilution, Serotec, Cedarlane Laboratories, Ontario, Canada), HRP-labeled anti-mouse IgG antibody (1:100 dilution, Sigma) and TSA-tetramethyl rhodamine (NEN Life Sciences, Boston, MA, USA). Samples were mounted as described above.

Devices were stained for GFAP and cell nuclei by treatment with 1% Triton X-100 in HBHS, and incubation with 5% bovine serum albumin (BSA) in HBHS to block non-specific binding, followed by rabbit anti-cow GFAP antibody (1:200 dilution, Sigma), biotin-conjugated anti-rabbit IgG antibody (BAR, 1:200 dilution, Sigma), Quantum-Red Streptavidin conjugate (1:20 dilution, Sigma) and CyQuant™ (1:30 000, Molecular Devices, Eugene, OR, USA). Samples were mounted in well slides as described above.

Preparation controls were prepared for each immunohistochemical run. These were processed without primary antibodies for all antigens tested. For TSA amplification, controls were also processed without secondary antibodies but did contain the TSA incubation step. All of these controls were negative for fluorescence. The presented results are representative of three or more tissue slices prepared from animals inserted with each type of device.

2.4. Imaging and image analysis

Images of the tissue and of devices labeled for cellular components were collected by confocal laser scanning microscopy using a Bio-Rad MRC600 or a NORAN confocal system mounted on Olympus IX-70 inverted microscopes using ×10 (0.40 NA) and ×40 (1.0 NA) objective lenses. The images were collected as three-dimensional stacks presented as maximum intensity value projections using Bio-Rad™, Intervision™ and Analyze™ software [38]. Images of the devices were also recorded using an ETEC scanning electron microscope in the secondary electron mode after coating the devices with gold in a sputter coater.

3. Results

All animals recovered from surgery with no apparent adverse effects and all survived for the duration of the experiment. No behavioral, or gross- or micro-pathology including infection were observed. Although CNF and CNCT devices were inserted using different methods, the overall insertion processes appeared to be equivalent.

3.1. GFAP-immunoreactivity around CNF and CNCT devices

GFAP-immunoreactivity is a standard measure used for assessing reactive gliosis [44,18,28,33,35]. Small, spindle-shaped GFAP-positive cells were presumed to be astrocytes and were scattered throughout control tissues. These cells were most frequently observed around larger blood vessels (data not shown).

One day post surgery, all insertion sites were characterized by non-uniform regions of increased diffuse fluorescence in a region 100–200 μm immediately around the device insertion sites (see Fig. 3, 1 day). At 1 week, all insertion sites showed an increase in number, size, and fluorescent intensity of GFAP-positive cells. GFAP-positive cells at the insertion sites from the larger CNF device sites were different from the CNCT device sites in two ways. First, the density of GFAP-positive cells immediately around the insertion sites was greater. Second, many of these cells had long processes projecting into the region surrounding the void created by withdrawal of the device. GFAP-positive cells around the CNCT device sites remained generally stellate but were clearly hypertrophied when compared to control cells. By 2 weeks, the intensity and number of GFAP-positive cells increased surrounding both device types. The cell morphologies were also similar. At this time the GFAP-positive cells began to become aligned around both types of device sites. At 4 weeks, a clear sheath of GFAP-positive astrocytes was observed. The thickness of the sheath at this time varied between 50 and 100 μm around the perimeter of the insertion site. An increased number of GFAP-positive stellate-shaped astrocytes were observed to a radius of about 500 μm from the insertion sites. In the images presented for 4 and 6 weeks post-insertion, the tissue preparation resulted in the data being collected at a bias relative to the inserted device, enabling us to describe the organization of cells at the device-tissue interface along one side of the insertion site. These images indicate that the compact sheath consists of a mesh of intertwined

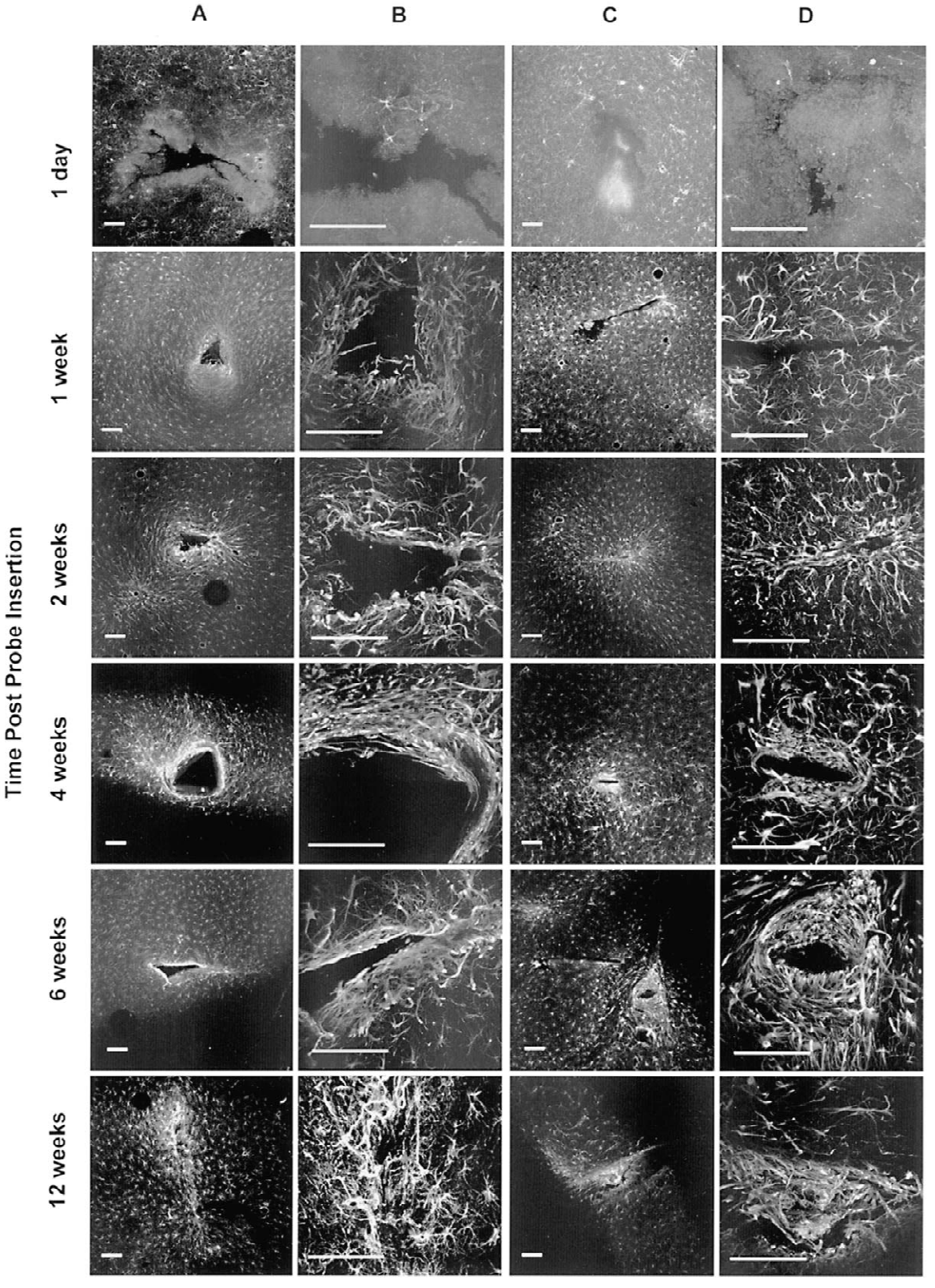

Fig. 3. GFAP immunohistochemistry of tissues slices from brains inserted with CNF, KOH-etched (columns A and B) and CNCT devices (columns C and D) at 1 day and 1, 2, 4, 6, and 12 weeks post insertion. Tissue slices were prepared as described in Section 2 and presented as maximum intensity projections. Images in columns A and C were obtained using a ×10 NA 0.4 objective lens, while images in columns B and D were obtained using a ×40 NA 1.0 objective lens. At 1 day post insertion diffuse GFAP staining is observed. By 1 week post-insertion hypertrophied, strongly labeled GFAP-labeled astrocytes were observed around insertion sites. Initially more of these cells are found around insertion sites made using CNF devices than CNCT devices; however, the responses look nearly identical 4 weeks after insertion. All scale bars=100 μm.

GFAP-positive processes. By 6 weeks, the sheath was thinner and more compact with fewer cells observed at greater distances from the insertion sites. The cell and sheath morphologies were similar for all animals. At 12 weeks, GFAP-positive reactivity surrounding the device sites was maintained remaining similar to that observed at 6 weeks. Again, the reactive responses observed were similar for both CNF and CNCT devices. Device removal frequently disrupted the structure of the sheath, resulting in individual process (see Fig. 3, 1 week, B) or larger numbers of processes and cells (see Fig. 3, 12 weeks, B and D) being pulled away from the brain parenchyma and into the void created when devices were withdrawn.

GFAP-immunohistochemistry described similar reactive responses to both the larger CNF and CNCT devices. However, the reactive responses observed at earlier times were larger for the CNF devices. Responses at longer times for both devices were similar indicating that they developed independent of device size, geometry, surface characteristics, and insertion method.

3.2. Vimentin immunoreactivity around CNF and CNCT devices

Vimentin expression is increased in reactive astrocytes and is not normally expressed in mature astrocytes [6,12,15,40]. In control brain regions vimentin was detected only in the ependymal lining of the ventricles (data not shown).

On day 1, vimentin was detected as small clusters of diffuse staining or in small amoeboid cells extending approximately 100 μm around device insertion sites. Similar responses were observed around both CNF and CNCT devices (see Fig. 4). At 1 week, the larger CNF device sites were surrounded by intensely stained vimentin-positive cell processes extending into and away from the void created by device withdrawal. These cells had long thin processes extending 100 μm and formed a loose thin layer around the device site in contrast to the much more abundant GFAP-positive cells. Insertion sites from CNCT devices appeared to have fewer and less intensely labeled vimentin-positive cells. By 2 weeks, the sites of both device types were similar in appearance. Vimentin-positive astrocytes with long, thin processes extending out 100–150 μm formed a layer around the device sites with the beginnings of a sheath. At 4 weeks, a compact sheath with intense vimentin-positive staining was observed. A thin layer (~25 μm) of less intensely vimentin-labeled cells can be seen in the space between the device and more intensely labeled and aligned vimentin-positive cells. The CNCT device sites were similar in appearance, but the vimentin-positive cells appeared to be less well organized. At 6 weeks, the extent and density of the vimentin-positive staining had decreased. Sites around both types of devices had a compact sheath of vimentin-positive astrocytes 50–100 μm. These astrocytes were well stained and had long, thin processes. At 12 weeks, both device types showed a thin highly compact 25–50 μm layer of vimentin-positive cells surrounding the device site. There was also a clear layer of less intensely labeled cells inside the more intensely labeled cells.

The vimentin-positive response to both device types was similar. As with GFAP-immunohistochemistry, the larger CNF devices produced responses in a larger volume of tissue at early times. A compact sheath of vimentin-positive cells was fully organized by 4 weeks and maintained for 12 weeks independent of device type and insertion method. Vimentin immunolabeling appeared to describe many fewer cells than GFAP immunolabeling.

3.3. ED1 immunoreactivity around CNF and CNCT devices

ED1 expression is an indicator of reactive microglia [4,19,27,36]. Observation of contralateral tissue confirmed that ED1 expression was more extensive in the immediate area around insertion sites.

On day 1, insertion sites created by both CNF and CNCT devices were characterized by an increase in the number of small, amoeboid ED1-positive cells in the surrounding tissue (see Fig. 5). At 1 week, all device sites showed an increase in ED1-positive microglia over an area three to four times the void left by device withdrawal. The ED1-positive microglia closest to the insertion site had short, thick processes, while cells a little further away from the void left by device removal were highly elongated. These insertion sites were also characterized by a thin layer of poorly stained cells immediately next to the device site. At 2 weeks, insertion sites were characterized by intense staining around the device site with a lumen filled

Fig. 4. Vimentin immunohistochemistry of tissues slices from brains inserted with CNF, KOH-etched (columns A and B) and CNCT devices (columns C and D) at 1 day and 1, 2, 4, 6, and 12 weeks post insertion. Tissue slices were prepared as described in Section 2 and images are presented as described for Fig. 3. At day one following insertion numerous small cells were observed around the insertion sites; however, some of this staining with CNCT devices may be extracellular (see 1 day, D). At 1 week the responses are much less robust around the CNCT devices. After 2 weeks the responses around both types of devices are similar. In general many fewer cells are observed using vimentin than GFAP. By 12 weeks the intensity and number of vimentin-positive cells is less than the number of GFAP-positive and there is some extracellular staining in the void left by withdrawal of the devices. The vimentin-positive band of cells seen near device sites in the 4, 6, and 12 week samples in Column C is associated with ependymal cells lining the ventricle between the cortex and hippocampus. These particular tissue slices were sufficiently deep that they begin to include portions of this structure. Ependymal cells were also stained in control tissue slices, and regions of the brain away from insertion devices, indicating that this labeling was independent of device insertion. All scale bars=100 μm.

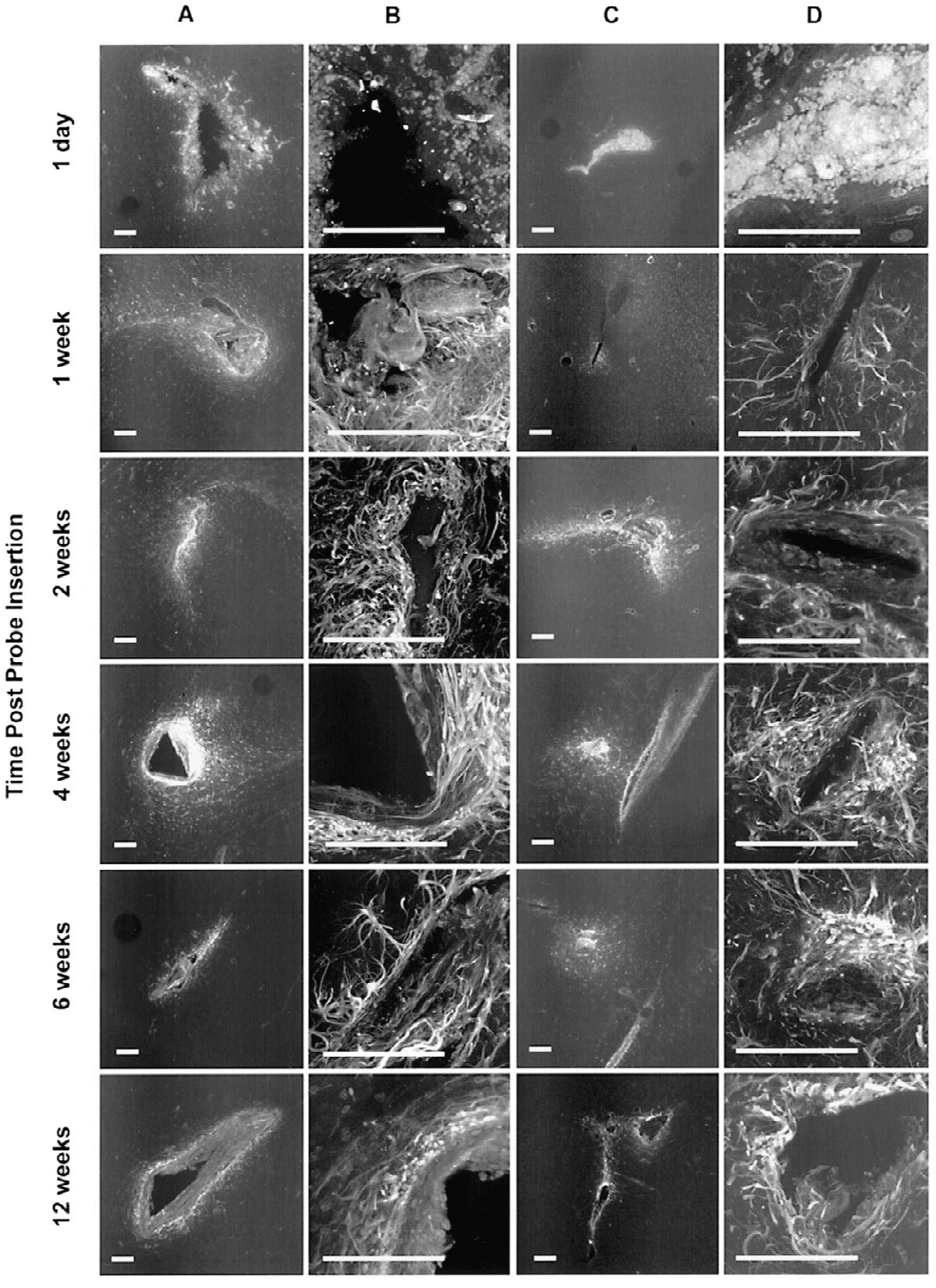
A
B
C
D
1 day
1 week
2 weeks
4 weeks
6 weeks
12 weeks
Time Post Probe Insertion

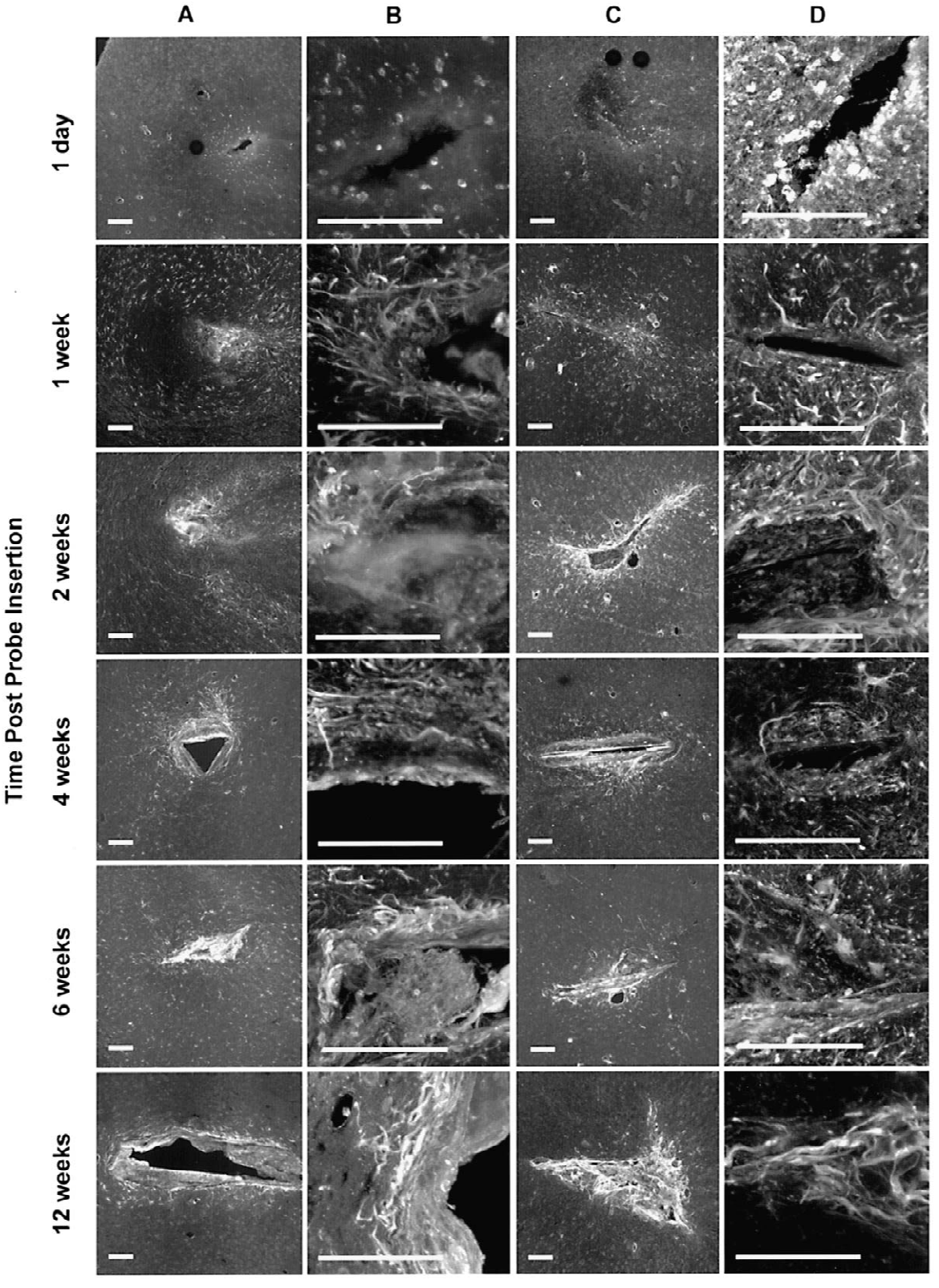

Fig. 5. ED1 immunohistochemistry of tissues slices from brains inserted with CNF, KOH-etched (columns A and B) and CNCT devices (columns C and D) at 1 day and 1, 2, 4, 6, and 12 weeks post insertion. Tissue slices were prepared as described in Section 2 and images are presented as described for Fig. 3. The number, distribution, and cell morphology of ED1-positive cells is similar in the insertion sites for both types of devices. A relatively small number of ameboid-looking cells were labeled 1 day following insertion. These cells became more numerous and spindle-shaped after 1 week. Many fewer ED1-positive cells were labeled than astrocytes labeled with either GFAP or vimentin. All scale bars=100 μm.

with diffusely stained material. At 4 weeks, both device sites showed ED1-positive staining surrounding a diffusely stained 100–200-μm thick layer. By 6 weeks, the ED1-positive cell layer was more compact for both device types. Additionally, diffusely stained material filled the lumen of both device sites. At 12 weeks, ED1-positive microglia formed a thin compact cell layer ensheathing a thick diffusely stained layer around the CNF device sites. The CNCT device insertion sites were surrounded by ED1-positive microglia that had collapsed into the lumen of the device site.

ED1-immunohistochemistry also demonstrated similar cellular responses to both devices. Variations observed at the earlier times correlated with the sizes of the devices. By 4 weeks responses were very similar. These data indicate that microglial responses, like astroglial responses, are independent of device type or method of insertion.

3.4. Immunoreactivity on CNF and CNCT devices removed at various times after insertion

Following tissue fixation but prior to sectioning, devices were gently removed by hand from the tissue, and were processed for immunohistochemistry similar to tissue slices. Devices were stained for GFAP and cell nuclei. Both device types showed a large number of adherent cells (see Fig. 6). While many of the cells adhering to the devices were GFAP-positive, many others were not as indicated by isolated Cy-Quant-stained nuclei. All of the devices had some cells adhering to their surfaces. The numbers of nuclei and amount of GFAP-positive material observed was highly variable and did not appear to correlate with device size, fabrication method, layer of cortex, or time after insertion. These results indicate that different kinds of cells rapidly attach to devices after insertion and some cells continue to remain closely attached to devices for as long as we have made observations.

3.5. Immunohistochemistry of insertion sites created by different sized CNF devices

These experiments were conducted to describe reactive responses around devices with shafts of different cross-sectional areas using our automated, microprocessor-controlled inserter, thus eliminating the variations associated with hand insertions. All of these devices were fabricated at the CNF, are of similar design and fabricated using similar methods. The cross-sectional area of the shafts were 16 900 μm^2 (Fig. 7, column A), 10 000 μm^2 (Fig. 7, column B), and 5000 μm^2 (Fig. 7, column C). These tissues were examined using GFAP immunohistochemistry and examined at 1 and 6 weeks following insertion. One week following insertion the number, distribution, and morphology of GFAP-positive cells was similar for the two device designs with larger cross-sectional areas. The responses observed around the devices with the smallest shanks appeared to involve fewer cells and closely resembled responses observed around CNCT devices (compare Fig. 7, images from 1 week columns A and B versus C and Fig. 3 images at 1 week) At 6 weeks the responses were very similar for all devices (see Fig. 7, 6 weeks row).

These observations indicate that the size of the device appears to be a principle factor in the volume of tissue and numbers of GFAP-positive cells that become involved in the reactive responses during the first week. This effect is independent of insertion method. The responses at 6 weeks are similar to all other devices.

4. Discussion

If neuroprostheses are to realize their full potential as tools to study the nervous system and as therapeutic devices used to restore CNS functions lost as a result of trauma or disease in humans, it is critical that devices and procedures be developed to minimize or eliminate the formation of the encapsulating sheath. One approach to this problem is to minimize the tissue damage at the time of insertion by making the prosthesis extremely small with smooth surfaces and rounded corners as previously suggested [17]. This approach assumes that the less damage created during insertion the better and that a smaller cross-section device will create less initial damage. Data presented here describe early (1 week or less) and sustained (2 weeks or longer) responses to devices with different sizes, surface characteristics, and insertion methods. The CNF devices with the largest shaft cross-sectional area (16 900 μm^2) had sharp corners and surface irregularities while devices with the smallest cross-sectional area (1450–2500 μm^2) had smooth surfaces and rounded corners. The smallest devices damaged less tissue, left a smaller hole when removed from the tissue, and initially produced a smaller volume of reactive tissue than larger devices. However, the sustained response of the brain to all implanted devices was the same and ultimately resulted in a compact cellular sheath containing astrocytes and microglia. While it is always best to minimize tissue damage on insertion, these results clearly indicate that the long-term tissue response is essentially the same, independent of prosthesis size, shape, surface texture and insertion method. Thus, these parameters do not influence the long-term functionality of devices implanted in the brain.

As previously demonstrated [44], reactive glia defined as GFAP-positive cells are a major component of the tissue reaction and the encapsulating sheath. The present study confirms the previously observed time course of sheath formation [44]. We have shown that the morphology and numbers of vimentin-positive cells appeared to be different from GFAP-positive cells. These probes may allow us to distinguish two different populations of astrocytes participating in the reactive responses, particularly the sus-

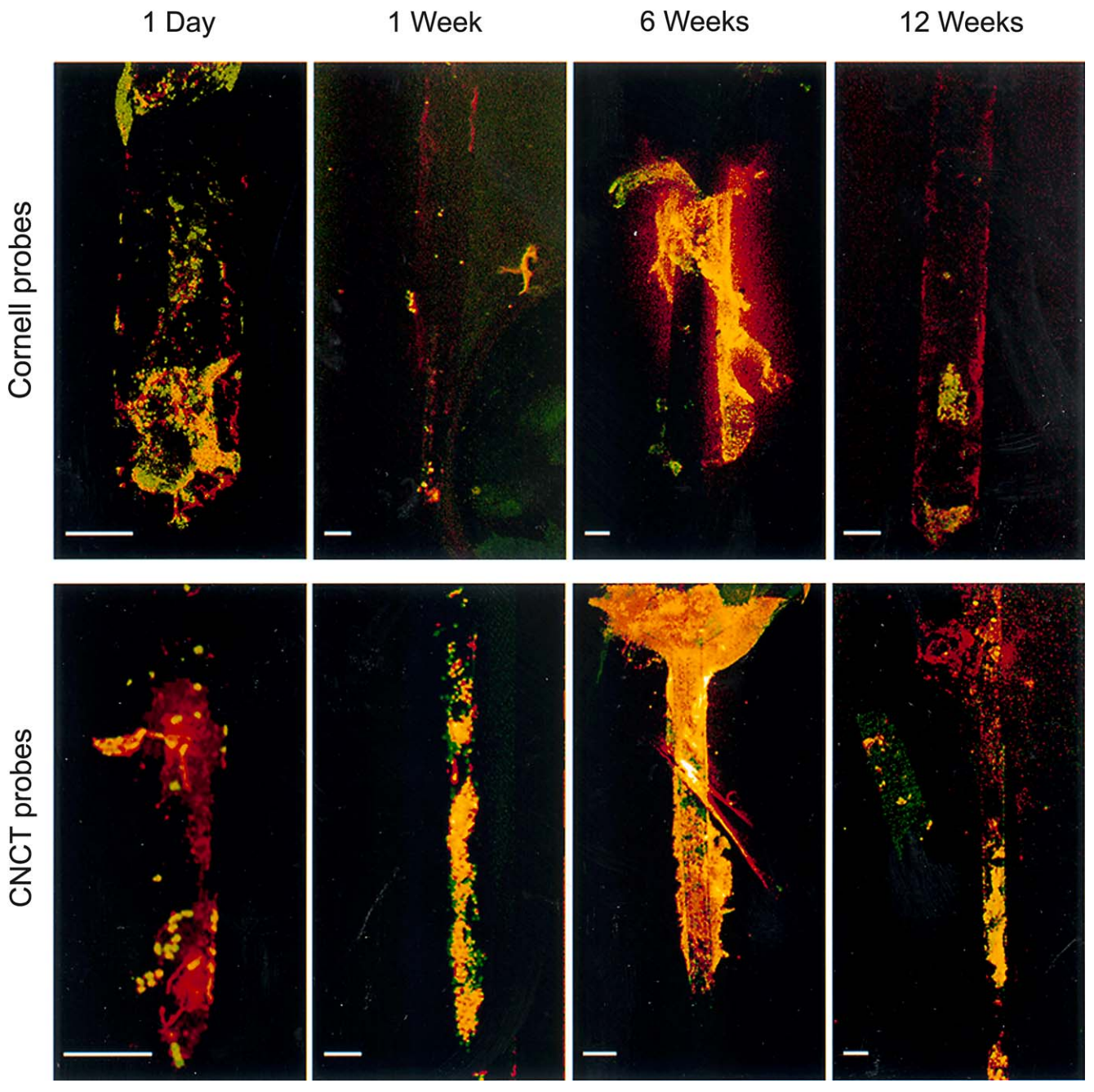

Fig. 6. GFAP-immunohistochemistry (red) and nuclear staining (green) of devices removed from brains at 1 day and 1, 6, and 12 weeks post insertion. Images are double-labeled and presented as maximum intensity projections. Devices were processed similarly to tissue slices as described in the Section 2. The amount of tissue associated with devices was variable and did not correlate with either type of device or period of time following insertion. While many nuclei were associated with GFAP-positive cells (yellow), many nuclei were not associated with GFAP-positive cells (green). These data demonstrate as early as 1 day following insertion a number of cells become attached to the surfaces of devices. Scale bars=100 μm.

tained responses observed after 4 weeks. Double label experiments designed using simultaneous analysis for GFAP and vimentin will further address this interpretation. ED1 staining demonstrates the localization of microglia to insertion sites and parallels the distribution and time course of GFAP at all time points from 1 day to 12 weeks. While the appearance of these cells is expected in the early times following insertion, it is interesting that these cells appear to be an important component of the reactive response and development of the cellular sheath even 6 and 12 weeks after device insertion. This observation suggests the sheath of cells is maintained by an active process resulting in continual activation of astrocytes and microglia.

Although CNF and CNCT devices had different surface characteristics, cells remained adherent to them after withdrawal from brain tissue. Two groups of cells were

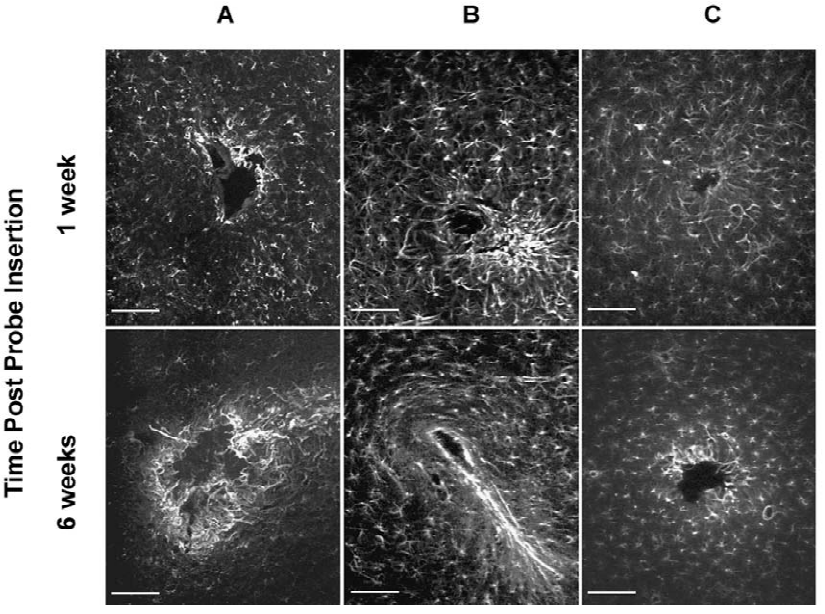

Fig. 7. GFAP immunohistochemistry of tissues slices from brains inserted with CNF, KOH (Column A)- and RIE (Columns B and C)-etched devices 1 and 6 weeks post insertion. The devices used in Column B had shafts with 100×100 μm cross-sectional dimensions. The devices in Column C had dimensions off 50×100 μm. Tissue slices were prepared as described in Section 2 and presented as maximum intensity projections. The responses observed are similar for all devices. However, the responses observed at 1 week for the smallest devices were not as extensive and did not affect as large a tissue volume as observed with the devices having larger shafts.

observed. Nuclear staining was used to differentiate GFAP-positive and -negative cells. The GFAP-negative cells may be microglia, cells derived from peripheral sources that entered the brain while the vasculature is damaged, or cells carried down from the pia during insertion. There was no correlation between the amount of material adherent to the devices and any experimental parameter. Further, there was no correlation between the appearance of broken cell processes in the lumen of the device sites with any experimental parameter. Therefore, cell attachment to devices and the presence of diffuse material in the lumen appear to occur randomly. A more complete investigation of the cells on devices is needed to make a clear identification.

Data presented here support our hypothesis that reactive responses observed after device insertion are of two types—an early reactive response observed immediately after device insertion, and a sustained reactive response that develops with time and is maintained long term [44]. Fig. 8 is a cartoon that depicts our current hypothesis of the mechanism of the reactive response. The early reactive response (Fig. 8A) may be the result of the insertion process itself, and may be initiated by damage to brain vasculature and other cells. Since we showed that the

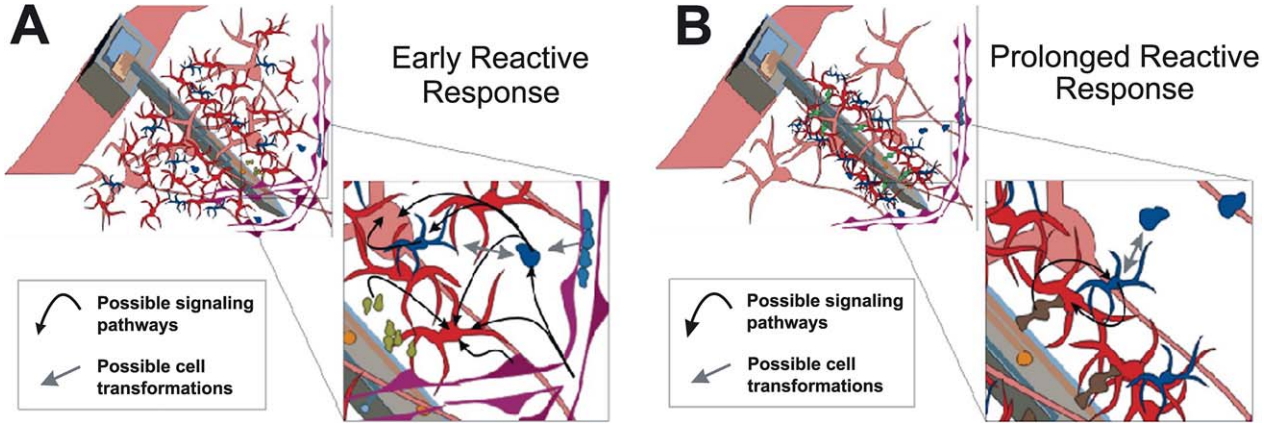

Fig. 8. Cartoons depicting cellular responses during early (A) and sustained (B) reactive responses observed following device insertion. The early response (A) is characterized by a large region containing reactive astrocytes and microglia around inserted devices. The sustained response (B) is characterized by a compact sheath of cells around insertion sites. Inserts depict potential cell–cell interactions and signaling pathways. Neurons (pink), astrocytes (red), monocyte derived cells including microglia (blue), and vasculature (purple) are depicted.

volume of tissue participating in this response is related to the cross-sectional area of device shafts, vascular damage and infiltration of cells from the periphery may play an important role in response initiation and development. Initial stages of this response observed within the first several days after insertion include an increase in GFAP and ED1 distribution indicating that significant cellular rearrangement may be occurring or cells may be activated in the immediate region. Vessels are ruptured and the number of reactive astrocytes and microglia increased throughout an extended volume Signaling pathways involving blood components, astrocytes, microglia, and endothelial cells are activated resulting in a molecular and cellular cascade. The sustained reactive response (Fig. 8B) may occur independently of the early reactive response since the characteristic distribution of cells around the insertion sites is independent of the magnitude of the early response. The hallmark of this response is the formation of a compact sheath around the devices such that all tissue, except that in the immediate vicinity of the sheath, appears similar to that observed in control brain regions. The reactive astrocytes and microglia occupy a much smaller tissue volume and are primarily in the sheath. Since the vasculature is now healed, signaling pathways to maintain the response are limited to the cellular components of the brain.

Future studies will further delineate the cell types involved in both phases of the tissue response. The relationship of microglia and astrocytes to each other and to the vascular endothelia are essential to understand. Since it is reasonable to assert that device insertion damages the vasculature, it is important to determine the time course of vascular repair. Finally, the fate of neurons near the insertion site must be investigated in detail. Edell et al. [17] demonstrated a kill zone around the insertion site. The major conclusion of the present work is that active intervention is needed to control the reactive response, heal the vasculature and rescue neurons. Miniaturization of devices will not suffice. We are investigating methods of drug delivery via the implant to pharmacologically treat the immediate volume of effected tissue. The required drugs will be administered through microfluidics and/or time release polymer coatings with entrapped drugs.

Acknowledgements

This work was partially supported by NIH, NCRR RR10957, and NS9-RO1-NS40977 and the Cornell Nanofabrication Facility, a node of the National Nanofabrication Users Network supported by the NSF. The authors thank the Center for Neural Communication Technology sponsored by NIH, NCRR grant P41-RR09754 for devices. The authors wish to acknowledge the contributions of Mr. Alan Hershenroder and Mr. William Abbt of the Wadsworth Center's Automation and Instrumentation department who designed and fabricated the device insertion device and Mr. J. Dilgen for help with manuscript preparation.

References

[1] W.F. Agnew, T.G. Yuen, R.H. Pudenz, L.A. Bullara, Electrical Stimulation of the brain IV ultrastructurural studies, Surg. Neurol. 4 (1975) 438–448.
[2] W.F. Agnew, T.G. Yuen, D.B. McCreery, L.A. Bullara, Histopathological evaluation of prolonged intracortical electrical stimulation, Exp. Neurol. 92 (1986) 162–185.
[3] F. Alesch, M.M. Pinter, R.J. Helscher, L. Fertl, A.L. Benabid, W.T. Koos, Stimulation of the ventral intermediate thalamic nucleus in tremor dominated Parkinson's disease and essential tremor, Acta Neurochir. 136 (1995) 75–81.
[4] J.A. Amat, H. Ishiguro, K. Nakamura, W.T. Norton, Phenotypic diversity and kinetics of proliferating microglia and astrocytes following cortical stab wounds, Glia 16 (1996) 368–382.
[5] M.D. Andersen, D.H. Szarowski, K. Stapleton, C. Castro, R. Davis, W. Shain, H.G. Craighead, M. Isaacson, J.N. Turner, Brain responses to insertion of nanofabricated silicon probes, Soc. Neurosci. Abstr. 23 (1997) 68.
[6] S.A. Baldwin, S.W. Scheff, Intermediate filament change in astrocytes following mild cortical contusion, Glia 16 (1996) 266–275.
[7] J.G. Banwell, G.H. Creasey, A.M. Aggarwal, J.T. Mortimer, Management of the neurogenic bowel in patients with spinal cord injury, Urol. Clin. North Am. 20 (1993) 517–526.
[8] T.E. Bell, K.D. Wise, D.J. Andersen, A flexible micromachined electrode array for a cochlear prosthesis, Sensors & Actuators A–Physical 66 (1998) 63–69.
[9] N. Bhadra, J.T. Mortimer, Extraction forces and tissue changes during explant of CWRU-type intramuscular electrodes from rat gastrocnemius, Ann. Biomed. Eng. 25 (1997) 1017–1025.
[10] S. Blond, J. Siegfried, Thalamic stimulation for the treatment of tremor and other movement disorders, Acta Neurochir. 52 (1991) 109–111.
[11] P. Bovolenta, F. Wandosell, M. Nieto-Sampedro, CNS glial scar tissue: a source of molecules which inhibit central neurite outgrowth, Prog. Brain Res. 94 (1992) 367–379.
[12] J.P. Bressler, N.A. Edwards, Glial shape and cytoskeletal protein synthesis, Neurochem. Res. 17 (1992) 173–177.
[13] D. Caparros-Lefebvre, S. Blond, N. Vermersch, J. Pecheux, J.D. Guieu, H. Petit, Chronic thalamic stimulation improves tremor and levodopa induced dyskinesias in Parkinson's disease, J. Neurol. Neurosurg. Psychiatry 56 (2002) 268–273.
[14] R.R. Carter, J.C. Houk, Multiple single-unit recordings from the CNS using thin-film arrays, IEEE Trans. Rehabil. Eng. 1 (1993) 175–184.
[15] F.-C. Chiu, J.E. Goldman, Synthesis and turnover of cytoskeletal proteins in cultured astrocytes, J. Neurochem. 42 (1984) 166–174.
[16] K.L. Drake, K.D. Wise, J. Farraye, D.J. Andersen, S.L. BeMent, Performance of planar multisite microdevices in recording extracellular single-unit intracortical activity, IEEE Trans. Biomed. Eng. 35 (1988) 719–732.
[17] D.J. Edell, V.V. Toi, V.M. McNeil, L.D. Clark, Factors influencing the biocompatibility of insertable silicon microshafts in cerebral cortex, IEEE Trans. Biomed. Eng. 39 (1992) 635–643.
[18] L.F. Eng, A.C.H. Yu, Y.L. Lee, Astrocytic response to injury, Prog. Brain Res. 94 (1992) 353–365.
[19] I. Fernaud-Espinosa, M. Nieto-Sampedro, P. Bovolenta, Differential activation of microglia and astrocytes in aniso- and isomorphic gliotic tissue, Glia 8 (1993) 277–291.

[20] W.M. Grill, J.T. Mortimer, Quantification of recruitment properties of multiple contact cuff electrodes, IEEE Trans. Rehabil. Eng. 4 (1996) 49–62.
[21] W.M. Grill, J.T. Mortimer, Inversion of the current-distance relationship by transient depolarization, IEEE Trans. Biomed. Eng. 44 (1997) 1–9.
[22] F.T. Hambrecht, The history of neural stimulation and its relevance to future neural prostheses, in: W.F. Agnew, D.B. McCreery (Eds.), Neural Prostheses, Prentice-Hall, Englewood Cliffs, NJ, 1990, pp. 2–23.
[23] W.J. Heetderks, F.T. Hambrecht, Applied neural control in the 1990's, Proc. IEEE 76 (1990) 1115–1121.
[24] J.F. Hetke, L.L. Lund, K. Najafi, K.D. Wise, D.J. Andersen, Silicon ribbon cables for chronically implantable microelectrode arrays, IEEE Trans. Biomed. Eng. 41 (1994) 314–321.
[25] A.C. Hoogerwerf, K.D. Wise, A three-dimensional microelectrode array for chronic neural recording, IEEE Trans. Biomed. Eng. 41 (1994) 1136–1145.
[26] J. Ji, K.D. Wise, An implantable CMOS circuit interface for multiplexed microelectrode recording arrays, IEEE J. Solid State Cir. 27 (1992) 433–443.
[27] M.A. Kahn, J.A. Ellision, G.J. Speight, J. de Vellis, CNTF regulation of astrogliosis and the activation of microglia in the developing rat central nervous system, Brain Res. 685 (1995) 55–67.
[28] D.M. Landis, The Early Reactions of non-neuronal cells to brain injury, Annu. Rev. Neurosci. 17 (1994) 133–151.
[29] E.M. Maynard, E. Fernandez, R.A. Normann, A technique to present dural adhesions to chronically implanted microelectrode arrays, J. Neurosci. Methods 97 (2000) 93–101.
[30] D.B. McCreery, W.F. Agnew, J. McHardy, Electrical characteristics of chronically implanted platinum-iridium electrodes, IEEE Trans. Biomed. Eng. 34 (1987) 664–668.
[31] D.B. McCreery, T.G. Yuen, W.F. Agnew, L.A. Bullara, A quantitative computer-assisted morphometric analysis of stimulation-induced injury to myelinated fibers in a peripheral nerve, J. Neurosci. Methods 73 (1997) 159–168.
[32] D.B. McCreery, T.G. Yuen, W.F. Agnew, L.A. Bullara, A characterization of the effects on neuronal excitable due to prolonged microstimulation with chronically implanted microelectrodes, IEEE Trans. Biomed. Eng. 44 (1997) 931–939.
[33] M.D. Norenberg, Astrocyte response to CNS injury, J. Neuropathol. Exp. Neurol. 53 (1994) 213–220.
[34] R.A. Normann, P.K. Campbell, W.P. LI, Silicon based microstructures suitable for intracortical electrical stimulation, IEEE J. Solid State Cir. (1988) 714–715.
[35] W.T. Norton, D.A. Aquino, I. Hozumi, F.-C. Chiu, C.F. Brosnan, Quantitative aspects of reactive gliosis: a review, Neurochem. Res. 17 (1992) 877–885.
[36] P.G. Popovish, P. Wei, B.T. Stokes, Cellular inflammatory response after spinal cord injury in Sprague–Dawley and Lewis rats, J. Comp. Neurol. 377 (1997) 443–464.
[37] H.J.P. Reitboeck, A 19-channel matrix drive with individually controllable fiber microelectrodes for neurophysiological applications, IEEE Trans. Syst. Man Cybernetics SMC –13 (1983) 676–683.
[38] R.A. Robb, C. Barillote, Interactive display and analysis of 3-D medical images, IEEE Trans. Med. Imaging 8 (1989) 217–226.
[39] P.J. Rousche, R.A. Normann, A method for pneumatically inserting an array of penetrating electrodes into cortical tissue, Ann. Biomed. Eng. 20 (1992) 423–437.
[40] D. Schiffer, M.T. Giodana, P. Caballa, M.C. Vigliani, A. Attanasio, Immunohistochemistry of glial reaction after injury in the rat: Double stainings and markers of cell proliferation, Neuroscience 11 (1993) 269–280.
[41] S. Schmidt, K. Horch, R. Normann, Biocompatibility of silicon based electrode arrays implanted in feline cortical tissue, J. Biomed. Mater. Res. 27 (1993) 1393–1399.
[42] S.S. Stensaas, L.J. Stensaas, The reaction of the cerebral cortex chronically implanted plastic needles, Acta Neuropathol. (Berlin) 35 (1976) 187–203.
[43] S.J. Tanghe, K.D. Wise, A 16-channel CMOS neural stimulating array, IEEE J. Solid-State Cir. 27 (1992) 1819–1825.
[44] J.N. Turner, W.G. Shain, D.H. Szarowski, M.D. Andersen, S. Martins, M. Isaacson, H.G. Craighead, Cerebral astrocyte response to micro-machined silicon implants, Exp. Neurol. 156 (1999) 33–49.
[45] D.J. Tyler, D.M. Durand, A slowly penetrating interfascicular nerve electrode for selective activation of peripheral nerves, IEEE Trans. Rehabil. Eng. 5 (1997) 51–61.
[46] B.J. Woodford, R.R. Carter, D. McCreery, L.A. Bullara, W.F. Agnew, Histopathologic and physiologic effects of chronic implantation of microelectrodes in sacral spinal cord of the cat, J. Neuropathol. Exp. Neurol. 55 (1996) 982–991.
[47] T.G. Yuen, W.F. Agnew, Histological evaluation of polyesterimide-insulated gold wires in the brain, Biomaterials 16 (1995) 951–956.